

Facile One-pot Exfoliation and Integration of 2D Layered Materials by Dispersion in a Photocurable Polymer Precursor

Alberto Gallardo, Jessica Pereyra, Enrique Martínez-Campos, Carolina García, David Acitores, Isabel Casado-Losada, Marián A. Gómez-Fatou, Helmut Reinecke, Gary Ellis, Diego Acevedo, Juan Rodríguez-Hernández, Horacio J. Salavagione*

1. *Full Experimental details*

Materials and methods

VP was distilled before use and stored at 4 °C. Graphite (Aldrich, < 45 micron, 99.99%, B.N. 496596-113.4G) and MoS₂ (Aldrich, < 2 micron, 99.99%) were used as received. Graphene and MoS₂ dispersions in VP were prepared by using an ultrasonic probe (Hielscher UP4005). Hydrogels were synthesized in a one-step conventional radical photopolymerization using 1-hydroxyl cyclohexyl phenyl ketone as initiator (0.5 wt. %). The reaction mixtures were bubbled with N₂ and transferred to polypropylene moulds via syringe, the moulds separated using 0.5 mm thick silicone spacers. The polymerization was undertaken during 40 minutes under UV radiation ($\lambda=365$ nm) from a UVP ultraviolet lamp (model CL-1000L, 230V). The networks were recovered from the moulds and were allowed to swell in Milli-Q water until equilibrium was reached. Subsequently, they were exhaustively washed with water to remove any soluble material. No graphene was detected in the washing solutions. The hydrogel precursor formulation developed was employed to create a 3D object using additive manufacturing (AM). The 3D hydrogel scaffold was designed using Autodesk Inventor 2015 and manufactured using a stereolithographic (SLA) printing technology. For that purpose, a Project 1200 3D printer from 3D systems was employed. The resolution achieved was 30 μm in z and around 56 μm (effective 585 dpi) in xy .

The cell studies were carried out using C166-GFP, a mouse endothelial cell line (CRL 2586™, obtained from ATCC®, USA) derived by transfection with a plasmid reporter vector,

pEGFP-N1, encoding enhanced green fluorescent protein (GFP). Routine passaging of the cell line was performed with DMEM high in glucose, supplemented with 10 % fetal bovine serum plus antibiotics. As a result of their self-fluorescence, they can be analysed through some non-opaque/translucent surfaces, such as the hydrogels employed here. Full details on the experimental protocol for cell culture experiments are provided in the ESI.

Equipment

UV/Vis absorption spectra of L2DM dispersed in VP were recorded on a Perkin Elmer Lambda 40 spectrophotometer.

Raman measurements were undertaken in the Raman Microspectroscopy Laboratory of the Characterization Service in the Institute of Polymer Science & Technology, CSIC using a Renishaw InVia-Reflex Raman system (Renishaw plc, Wotton-under-Edge, UK), which employed a grating spectrometer with a Peltier-cooled CCD detector coupled to a confocal microscope. The Raman scattering was excited with an argon ion laser ($\lambda = 514.5$ nm), focusing on the sample with a 100x microscope objective (NA=0.85) with a laser power of approximately 2 mW at the sample. Spectra were recorded in the range between 1000 and 3200 cm^{-1} . All spectral data was processed with Renishaw WiRE 3.2 software.

High-resolution transmission electron microscopy (HRTEM) analysis was conducted at the Centro Nacional de Microscopía Electrónica, Madrid, Spain. TEM micrographs were taken at random locations across the grids, to ensure a non-biased assessment. For measurement of graphene flake lateral dimensions and thickness, high-resolution HRTEM micrographs were performed on a JEOL JEM-2100 instrument (JEOL Ltd., Akishima, Tokyo, Japan), using a LaB6 filament, a lattice resolution of 0.25 nm and an acceleration voltage of 200 kV. Samples were prepared by drop-casting a few millilitres of dispersion onto holey carbon films (copper grids) and dried at 120 °C under vacuum for 12 hours.

The morphology of the nanocomposites was also examined by TEM performed at CAT, Universidad Rey Juan Carlos. Images were obtained with a Philips Tecnai 20 microscope. Ultrathin sections, 50–100 nm in thickness, were cryogenically microtomed with a diamond

knife at approximately $-60\text{ }^{\circ}\text{C}$ and supported on Cu TEM grids. Collecting images was not a straightforward task due to the poor stability of the polymeric gels under the electron beam.

2. *Graphene and MoS₂ dispersion and characterization.*

The solubility of layered materials has been fully studied.^[1] Firstly the surface energy (γ) was proposed as the principal factor influencing the degree of dispersion since the enthalpy of mixing ΔH_{mix} is directly related to the difference between the surface energy of the solute and the solvent. Therefore, it was proposed that the lower the difference γ between solute and solvent, the lower the ΔH_{mix} and, consequently, the higher the concentration of dispersed particles. The values of γ (in $\text{mN}\cdot\text{m}^{-1}$) for graphene,^[2] MoS₂^[3] N-vinylpyrrolidone (VP) and N-methylpyrrolidone (NMP) are represented in **Figure S1a** (left, red y-axis). It can be noted that the value for VP is closer to graphene than that of NMP. Therefore, similar or better dispersion of graphene may be expected. In addition, NMP is expected to disperse MoS₂ better than VP.

However, it has been reported that solvents with γ close to that of L2DM did not disperse these layered 2D materials (L2DM) and other criteria need to be considered, such as the Hildebrand solubility parameter (δ_{T}).^[4] The δ_{T} values presented in Figure S1A (right, blue y-axis), shows that all values fall in a short interval, and no significant difference between solvent and solute exist, suggesting that VP could be as good a solvent as NMP. However, the $\Delta\delta_{\text{T}}$ varies in the opposite sense to $\Delta\gamma$, suggesting that VP may be a slightly better solvent for MoS₂ and slightly worse for graphene than NMP.

In order to further understand this difference, a deeper insight can be obtained via a molecular-level approach using the Hansen solubility parameters. It is known that the δ_{T} can be divided into specific types of solute-solvent interactions, e.g. the Hansen solubility parameters of dispersion δ_{D} , polar (δ_{p}) and H-bonding (δ_{H}) interactions.

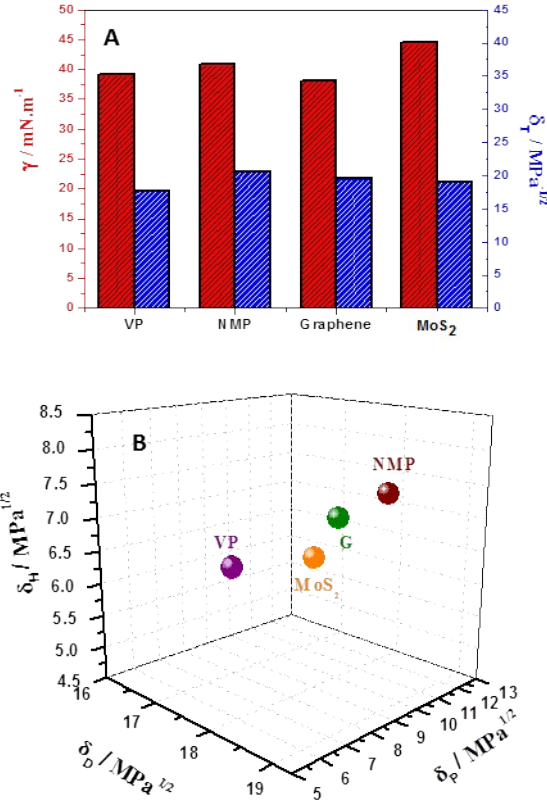


Figure S1. (A) Surface energy (γ) and Hildebrand solubility parameter (δ_T) and (B) an axiometric Hansen solubility plot for the L2DM and solvents studied in this work.

Values for the Hansen solubility parameters of $\delta_D \approx 18.0 \text{ MPa}^{1/2}$, $\delta_P \approx 10 \text{ MPa}^{1/2}$ and $\delta_H \approx 7 \text{ MPa}^{1/2}$ for graphene [5] and $\delta_D \approx 17.8 \text{ MPa}^{1/2}$, $\delta_P \approx 9 \text{ MPa}^{1/2}$ and $\delta_H \approx 7.5 \text{ MPa}^{1/2}$, for MoS_2 have been reported.[6] The polar contribution for VP ($\delta_D \approx 9.3 \text{ MPa}^{1/2}$) matches very well that for graphene and MoS_2 , while the other contributions slightly differ. Figure S1B shows a 3D representation of how the VP and NMP compare to graphene and MoS_2 from their distance in the Hansen space. This is the distance (R_a) between the vector from the point in Hansen space representing the solute and the solvent can be determined by equation:

$$R_a = \sqrt{4(\delta_{D,L2DM} - \delta_{D,solv})^2 + (\delta_{P,L2DM} - \delta_{P,solv})^2 + (\delta_{H,L2DM} - \delta_{H,solv})^2}$$

,with δ_{L2DM} and δ_{solv} representing each Hansen parameter for the particles and solvents, respectively. The distance in Hansen space is almost the same for the mixing of both solvents with MoS₂, but in the case of graphene R_a is significantly lower for NMP, suggesting that it performs better in this case. However, the Flory-Huggins parameter, χ , has also been proposed as a measure of the cost of mixing solvents and similar L2DM, and the lower the value of χ , the lower the energetic cost of dispersing L2DM.[4] This factor can be expressed as a function of the Hansen solubility parameters as follows:

$$\chi = \frac{v_0}{R.T} [(\delta_{D,L2DM} - \delta_{D,solv})^2 + (\delta_{P,L2DM} - \delta_{P,solv})^2 + (\delta_{H,L2DM} - \delta_{H,solv})^2] \quad \text{Eq. 1}$$

, where v_0 is the molar volume of the solvent in cm³.mol⁻¹, R the gas constant (8.31 cm³.Mpa.K⁻¹.mol⁻¹) and T the temperature in Kelvin. Using this expression, χ adopts similar values for both solvents in the case of graphene, albeit slightly lower for VP. But for MoS₂, VP presents a much lower χ value.

Table S1. List of solubility parameters used to estimate the potential of VP to disperse L2DM.

Material	δ_D (MPa ^{1/2})	δ_P (MPa ^{1/2})	δ_H (MPa ^{1/2})	Mixture	R_a (MPa ^{1/2})	χ
NMP	18	12.3	7.2	Gr, NMP	2.3	0,21
VP	16.4	9.3	5.9	Gr, VP	3.4	0.18
Graphene	18	10	7	MoS ₂ ,NMP	3.3	0.43
MoS ₂	17.8	9	7.5	MoS ₂ , VP	3.2	0.19

Despite the disparity in the predicted performance of NMP and VP for dispersing L2DM described above, it seems clear that the differences are not that significant and we expect that reasonable good concentrations of L2DM will be achieved in VP.

In order to optimize the dispersion conditions, a series of samples were prepared varying dispersion parameters such as initial graphite concentration (C_i), sonication time (S_i) and type

(pulsed, $S_{t,p}$ or continue, $S_{t,c}$) and centrifugation speed (V_c). Details on all samples evaluated are shown in **Table S2**. For all samples the nomenclature used takes the form XYYZZ, where X denotes the type of treatment, either C = continuous or P = pulsed ultrasound. YY refers to the initial concentration of graphite in mg.mL^{-1} and ZZ relates to the time of treatment in minutes.

Table S2. Experimental details and names for all samples studied in this work.

Sample	L2DM	Type ($S_{t,x}$)	C_i mg.mL^{-1}	(S_t) min	V_c kr.p.m.	[L2DM. mg.mL^{-1}
P0505	Gr	pulsed	5	5	7	0.004
P0515	Gr	pulsed	5	15	7	0.009
P0530	Gr	pulsed	5	30	7	0.02
P0560	Gr	pulsed	5	60	7	0.09
C2015	Gr	continuous	20	15	7	0.05
C2030	Gr	continuous	20	30	7	0.15
C2060	Gr	continuous	20	60	7	0.40
P0515	Gr	Pulsed	5	15	7	0.009
P1015	Gr	Pulsed	10	15	7	0.012
P2015	Gr	Pulsed	20	15	7	0.04
P5015	Gr	pulsed	50	15	7	0.12
C2030-Mo	MoS ₂	continuous	20	30	7	0.009

Figure S2 presents typical UV-visible spectra of graphene and MoS₂ dispersed in VP. The absorption spectrum of dispersed graphene is, in all cases, flat and featureless in the visible region as expected for quasi two-dimensional materials.^[2] In addition, the observed scattering effect is indicative of a dispersion containing non-aggregated ultrathin nanostructures. In the case of MoS₂, the two typical characteristic absorption peaks are clearly observed at 612 and 670 nm, assigned to the A1 and B1 direct exciton transitions of transition metal dichalcogenides, originated from the energy split valence-band and spin-orbital coupling. These two peaks indicate that the MoS₂ is dispersed in VP as the 2H-phase.^[7]

The molar extinction coefficient (ϵ) for Gr and MoS₂, dispersed in VP was experimentally determined. It takes values of $\epsilon_{660} = 1880 \text{ L.g}^{-1}.\text{m}^{-1}$ and $\epsilon_{672} = 2200 \text{ L.g}^{-1}.\text{m}^{-1}$ for Gr and MoS₂, respectively in good agreement with values in NMP.

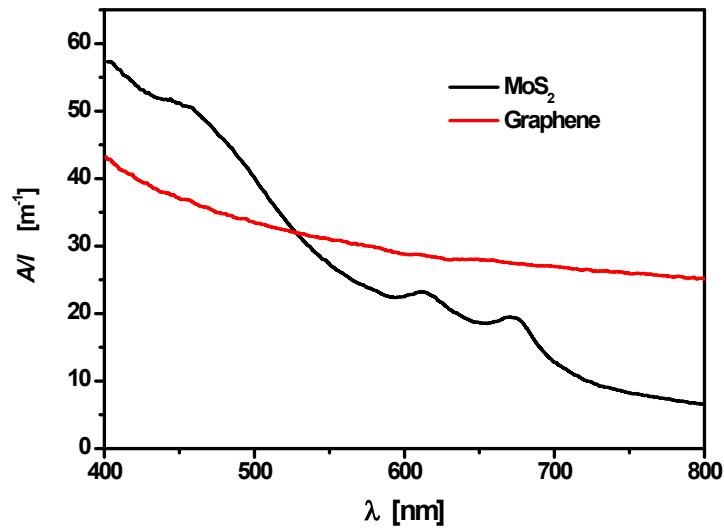


Figure S2. Absorption spectra of graphene (C2030) and MoS₂ (C2030-Mo) in VP.

As mentioned in main text, the concentration of dispersed graphene depends on the initial concentration of graphite, and time and type of ultrasound. In the case of the initial graphite concentration ($S_{t,p} = 15$ min; $V_c = 7$ kr.p.m.), a linear dependence is observed at lower initial concentrations (up to $C_i = 20$ mg.mL⁻¹), which is described by the expression $[C_{Gr}] = 1,28 \times 10^{-3} [C_i]$. The effect of sonication time ($C_i = 5$ mg.mL⁻¹; $V_c = 7$ kr.p.m.) strongly depends on the regime applied; pulsed sonication generated an increase in C_{Gr} described with the following expression: $[C_{Gr}] = 5 \times 10^{-4} [S_{t,p}]$, while the dependence of the graphene concentration for a continuous sonication regime can be adjusted with a more complex empirical formula: $[C_G] = 0.16 \cdot \exp(-5 \cdot \exp[-0.1[S_{t,c}]])$. The differences in the efficiency of graphene exfoliation between both methods are due to a strong decrease of the rate of cavitation zone development in the pulsed experiment. For molybdenum disulfide ($C_i = 20$ mg.mL⁻¹; $S_{t,c} = 30$ min; $V_c = 7$ kr.p.m.), using the experimentally measured molar coefficient extinction in VP of 2200 L.g⁻¹.m⁻¹ (at 672 nm), a concentration of 9.3×10^{-3} mg.mL⁻¹ was calculated (see Figure S2). However, this concentration could be improved by optimizing the dispersion parameters.

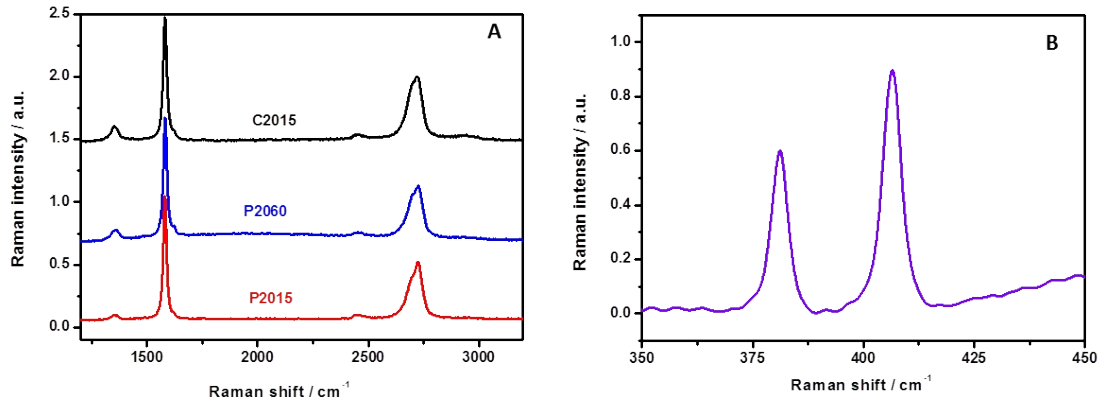


Figure S3. Representative Raman spectra of (A) different graphene and (B) MoS₂ (C2030-Mo) samples drop-cast from VP dispersions.

Representative Raman spectra for different samples of graphene and MoS₂ drop-cast from VP dispersions are shown in **Figure S3**. Graphene samples present the typical Raman features consisting of the G band at around 1582 cm⁻¹, the second order 2D band at around 2700 cm⁻¹ and the disorder-induced D band and edge-defect D' band at 1352 cm⁻¹ and 1622 cm⁻¹, respectively (Fig. S3A). The Raman spectrum of MoS₂ (C2030-Mo) shows strong signals from both the in-plane E_{1g}¹ and the out-of-plane A_{1g} vibration consistent with a trigonal prismatic (2H) phase (Fig. S3B).^[8] It has been reported that these peaks are sensitive to the thickness of the sample and that the difference between the maximum Raman shift for each peak increases with the number of layers. In our case the difference of ~ 25 cm⁻¹ between peak maxima resembles that for bulk MoS₂, but this is due to aggregation during the casting procedure. As NMP, VP evaporates slowly - and not completely - allowing the sheets to restack.

From Fig S3A it can be noted that the intensity ratio of D and G bands depends on the experimental conditions. The I_D/I_G intensity ratio has been used to estimate some crystallite parameters like the crystallite size L_a, which can be expressed as follows:^[9]

$$L_a(\text{nm}) = 2.4 \times 10^{-10} \lambda_l^4 \left(\frac{I_D}{I_G} \right)^{-1} \quad \text{Eq. 2}$$

where λ is the laser wavelength in nm, in this work 514.5 nm (2.41 eV). The variation of L_a with the experimental conditions for all samples is represented in Figure S4a, where a clear dependence with the sonication type and time is noted; the longer the sonication time, the lower L_a , being more evident for continuous treatment. A value of 72 ± 15 nm for 30 minutes of continuous treatment is obtained, which is similar to previously reported data.^[10] However, when varying the initial concentration of graphite L_a increases at low concentrations and then decreases.

The quality of the laminates can also be quantified based on the distance between defects (L_D) and the defect density (n_D), which can also be estimated from the I_D/I_G ratio using experimentally determined equations.^[11] The L_D can be expressed as:

$$L_D^2(nm^2) = (1.8 \pm 0.5) \times 10^{-9} \lambda_l^4 \left(\frac{I_D}{I_G} \right)^{-1} \quad \text{Eq. 3}$$

whereas n_D can be written as a function of I_D/I_G as follows:

$$n_D(cm^{-2}) = \frac{(1.8 \pm 0.5) \times 10^{22} \left(\frac{I_D}{I_G} \right)}{\lambda_l^4} \quad \text{Eq. 4}$$

The variation of L_D and n_D is shown in Figure S4 b and c, respectively. For continuous ultrasound for 30 minutes (C2030), the estimated values are 23 ± 2 nm and $6.32 \times 10^{10} \pm 1.44 \times 10^{10}$ for L_D and n_D , respectively, also resembling the results for polymer-assisted dispersed graphene.^[11]

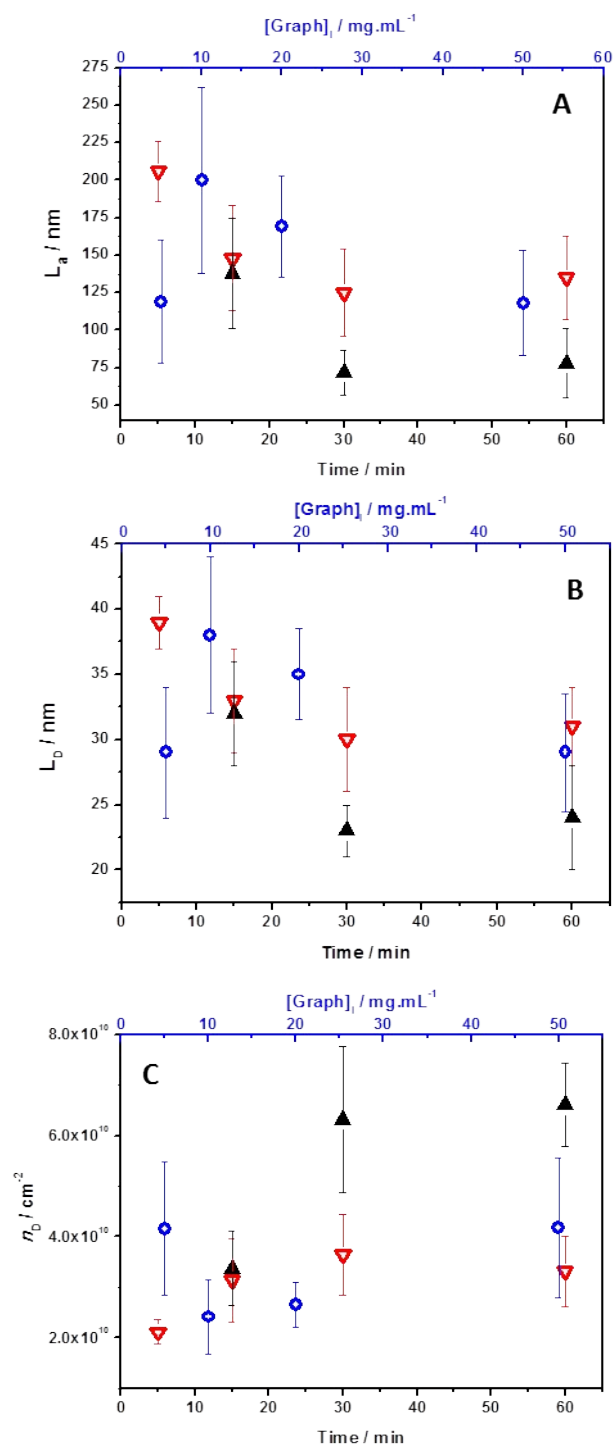


Figure S4. Variation of quality parameters of graphene dispersed in VP prepared under different experimental conditions. (A) Crystallite size, L_a , (B) distance between defects (L_D), and (C) the density of defects (n_D). Blue circles (top x -axis) correspond to variation of C_i ($S_{t,p} = 15$ min, $V_c = 7\text{kr.p.m}$). Effect of sonication time under pulsed (red triangles; $C_i = 5 \text{ mg.mL}^{-1}$; $V_c = 7\text{kr.p.m}$) and continuous (black triangles; $C_i = 20 \text{ mg.mL}^{-1}$; $V_c = 7\text{kr.p.m}$) treatments are referred to bottom x -axis.

Dispersed L2DM were also characterised by TEM (Figure S5). In both cases, graphene and MoS₂, samples prepared by 30 min continuous ultrasound treatment were thoroughly analysed. In the case of graphene a good concentration of 2D laminates was observed, with flakes of different lateral dimensions and thicknesses, was observed (Figure S5 A-C). MoS₂ also presents flakes of different dimensions and thickness, but the lateral dimensions are much smaller than those of case of graphene, with average length and width of 295 ± 60 nm and 148 ± 15 nm, respectively. The composition of the laminates was confirmed by energy-dispersive X-ray spectroscopy (EDX) that showed the presence of sulphur and molybdenum in a ratio of S:Mo of 67.12:32.88, matching perfectly the stoichiometry.

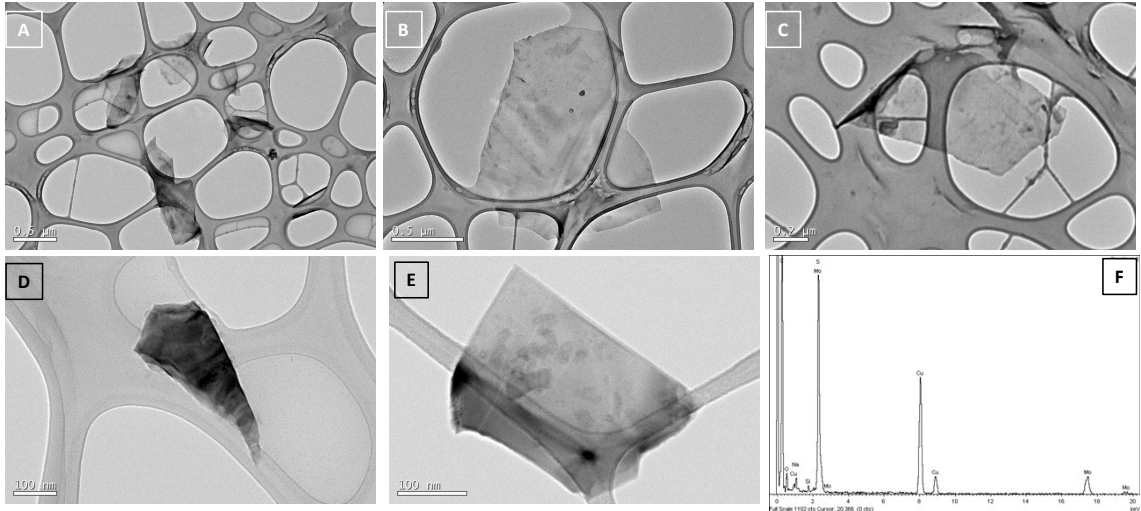


Figure S5. HRTEM characterization of dispersed L2DM. Representative TEM images of (A-C) Gr and (D, E) MoS₂ from VP dispersions, and (F) EDX analysis of the flake in E.

Recently, spectroscopic metrics have been reported to be useful to determine lateral dimensions of flakes according to the following expression:^[12]

$$\langle L \rangle = 50 \times e^{-0.21 \times \Gamma_G} \quad \text{Eq. 5}$$

where the mean size ($\langle L \rangle$) directly depends on the FWHM of the G band (Γ_G).

Figure S6 shows the variation of $\langle L \rangle$ as a function of the experimental parameters. It can be seen that $\langle L \rangle$ increases as C_i increases in a linear manner for $C_i \leq 20 \text{ mg.mL}^{-1}$. The variation of $\langle L \rangle$ with sonication time shows significant differences depending on whether continuous or pulsed treatment is applied. While in the former case $\langle L \rangle$ strongly decreases with $S_{t,c}$, for pulsed ultrasound $\langle L \rangle$ did not change with time.

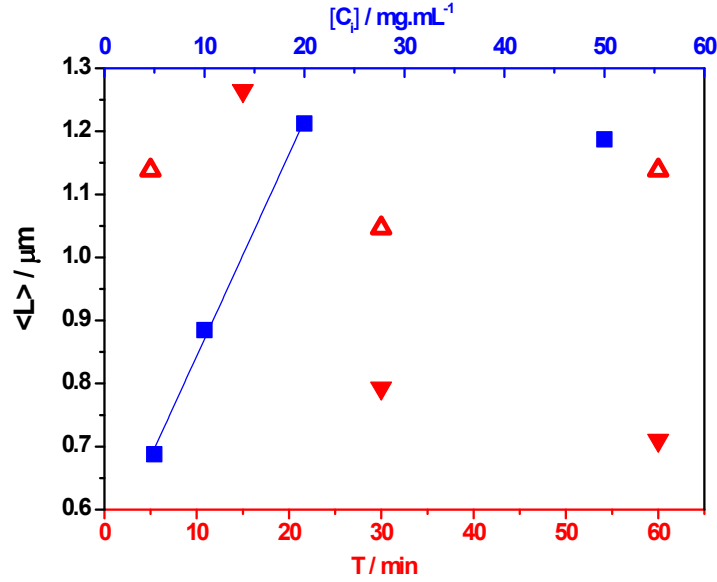


Figure S6. Variation of the mean size $\langle L \rangle$ of Gr flakes obtained from Raman spectra for samples prepared under different experimental conditions. Blue squares (top x -axis) correspond to variation of C_i ($S_{tp} = 15 \text{ min}$; $Vc = 7\text{kr.p.m}$). Effect of sonication time under pulsed (hollow red triangles; $C_i = 5 \text{ mg.mL}^{-1}$; $Vc = 7\text{kr.p.m}$) and continuous (filled red triangles; $C_i = 20 \text{ mg.mL}^{-1}$; $Vc = 7\text{kr.p.m}$) treatments are referred to bottom x -axis.

Spectroscopic metrics can also be used to determine the average number of layers ($\langle N \rangle$) as recently proposed^[13] In this case the shape of the 2D band, normalized with respect to the starting graphite used, is considered. The dependence of $\langle N \rangle$ with the 2D shape can be expressed as:

$$\langle N \rangle \geq 0.83 \times e^{3.6 \frac{[I_{\omega 1}/I_{\omega 2}]_{G'ene}}{[I_{\omega 1}/I_{\omega 2}]_{G'ite}}} \quad \text{Eq. 6}$$

where ω_1 and ω_2 are the intensity of the 2D band at maximum and the intensity 30 cm^{-1} below the maximum (shoulder), respectively. The suffix G'ene and G'ite refers to the graphene sample and starting graphite, respectively. Although the use of this equation has its limitations, we observed that the mean thickness of samples does not change with $S_{t,p}$, obtaining values between 10-12 layers. In the case of $S_{t,c}$ there is a clear effect of type and treatment time, and the sample prepared via 30 min continuous sonication presents a value of $\langle N \rangle$ of $\sim 3.15 \pm 0.75$ layers.

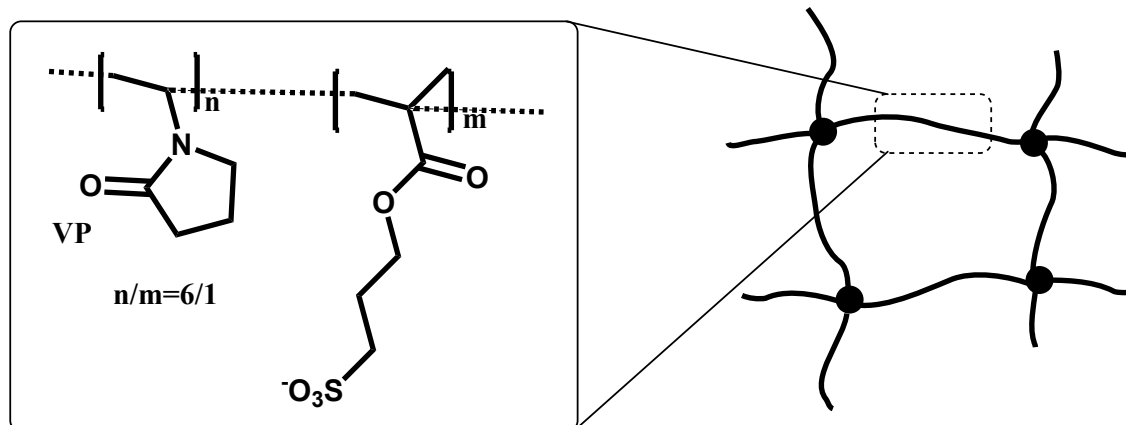
3. *PVP-based hydrogel nanocomposites.*

Polyvinylpyrrolidone (PVP) is a non-ionic amphiphilic polymer, soluble in water and in many organic solvents (it is used as polymeric surfactant) and non-toxic; PVP-based polymers have a broad range of applications and have been approved by the FDA for use as food additives (<http://www.accessdata.fda.gov/scripts/cdrh/cfdocs/cfcfr/CFRSearch.cfm?fr=173.55>, 2017). It has a large range of technological and biomedical applications. The incorporation of VP to polymeric networks, such as the VP-based membranes obtained by photocuring, imparts to the material different capabilities such as the mentioned non-toxicity, antifouling properties^[13,14,15] or capacity for water uptake, forming hydrogels. Hydrogels are soft materials highly interesting in biomedicine due to their hydration process, resembling that of some natural tissues, and biocompatibility.^[16] As an example, classic contact lenses were VP-based membrane hydrogels.

Our group has recently reported on the preparation of VP- based hydrogels with pseudo-double network (pseudo-DN) structure and unique properties for cell manipulation.^[17] These PVP supports allowed cells to grow to confluence, and subsequently rapid cell detachment could be induced through simple mechanical agitation. Subsequently, the resulting cell sheets could be easily transplanted without the need for a cell superstrate. The materials were prepared via simple one step radical photocuring and were in the hydrated state, robust and easy to manipulate in spite of a high water content $> 80\text{ wt. \%}$. The term pseudo-DN refers to the structural tendency of these materials to form DN_s,^[18] which can be described as interpenetrating polymer networks (IPNs) comprised of two highly asymmetric crosslinked

networks. DNs have been reported to exhibit astonishing mechanical properties in the high swollen state.^[19]

Hydrogels were prepared according to the protocol previously reported,^[18] described in the experimental section of the main text (Scheme S1). A summary of the hydrogel types prepared is given in Table S3.



Scheme S1. Main components of the networks: vinylpyrrolidone (VP) and sulfopropylmethacrylate, crosslinked with an optimized mixture of two crosslinkers as indicated in Experimental Section.

The distribution of graphene in the hydrogel membranes has been evaluated by TEM (Figure 2, main text and Figure S7)

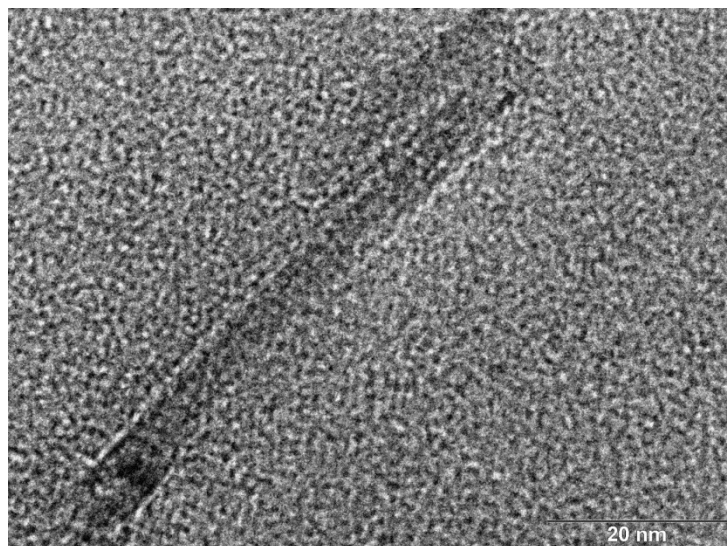


Figure S7. HRTEM image showing the graphene laminates into the polymer hydrogel.

The properties of hydrogel nanocomposites were evaluated by several experimental techniques. Swelling experiments were performed gravimetrically in distilled water. The samples were allowed to swell for one day to allow for equilibrium swelling. The swelling degree was determined according to the following expression:

$$S (\%) = \frac{W_t - W_0}{W_t} \cdot 100 \quad \text{Eq.7}$$

where W_t and W_0 are the weights of the swollen and dried sample, respectively.

As mentioned in the main text, this feature, very important for hydrogel materials, remains constant for all studied samples, indicating no negative effect of the L2DM, in principle expected for hydrophobic graphene.^[20]

The surface wettability of the hydrogels was measured by the capillary rise technique.^[21] A 0.3 cm x 2 cm hydrogel monolith was placed vertically over an aqueous solution. When the hydrogel contacts the surface of the water a capillary quickly rises up the hydrogel.^[22] According to the literature the height of the meniscus is an indirect measurement of the

hydrophilicity of a plate, in this case the hydrogel.^[23] The height of the capillary rise h can be measured and by integration of the Laplace equation^[24] the following equation results:

$$\sin \theta = 1 - \frac{\Delta\rho gh^2}{2\gamma_{lv}} \quad \text{Eq. 8}$$

where $\Delta\rho$ is the difference in density between the liquid (water in this case 1000 kg/m³) and vapor (air 1.09 kg/m³), g is the acceleration due to gravity (9,8 m/s²) and γ_{lv} is the liquid surface tension (72.75 mN/m² for water), h is the capillary rise and θ is the contact angle. Thus, a direct measurement of the capillary rise can be employed to calculate the contact angle. The temperature of the water solution was maintained constant at 25°C. The principal results of this analysis are discussed in the main text.

Mechanical properties were measured by dynamic compression tests on equilibrium water-swollen gels at 25 °C in a MTS® QTest1/L Elite testing machine equipped with a 10 N load cell in compression mode. All hydrogel samples were prepared in a 6 mm diameter cylindrical form. Samples were completely immersed in a water bath and placed between compression platens; the upper one is 5 mm of diameter. Each sample was subsequently deformed at 0.1 mm.min⁻¹. To obtain statistically reliable results all measurements were performed on 5 test specimens for each hydrogel system. As an example **Figure S7** shows the compression curves obtained for the sample P0560/VP in the hydrated state. The modulus was calculated in the linear region at lower deformations, where the material follows Hooke's law.

Modulus, stress and strain at break for almost all nanocomposite hydrogels are in the same order as the neat polymer hydrogel, suggesting no significant effect of the L2DM, except for the sample containing MoS₂, as discussed in the main text. The sample with the highest amount of graphene shows the lowest modulus value, which can be due to poorer dispersion of graphene. In fact some aggregates were observed with an optical microscope. However, a negative effect during the in-situ photo-curing process should not be discarded and more experiments are planned to check this possibility.

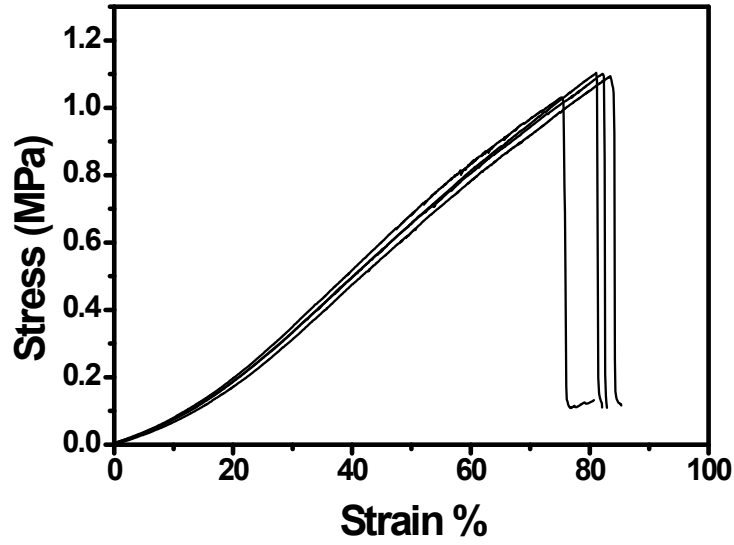


Figure S8. Example of Stress-Strain curves obtained by compression test of hydrated P0560/VP samples.

Mesh size ξ has been determined from the swelling data by using the methodology described by Carr and Peppas for PVP-based hydrogels, which need these two equations:^[25]

$$\frac{1}{\overline{M}_c} = \frac{2}{\overline{M}_n} - \frac{\left(\frac{\bar{v}}{V_1}\right) \left[\ln(1 - v_{2,s}) + v_{2,s} + \chi v_{2,s}^2 \right]}{v_{2,r} \left[\left(\frac{v_{2,s}}{v_{2,r}}\right)^3 - \frac{v_{2,s}}{2v_{2,r}} \right]} \quad \text{Eq. 9}$$

$$\xi = v_{2,s}^{-1/3} \left(\frac{2C_n \overline{M}_c}{M_r} \right)^{1/2} l \quad \text{Eq. 10}$$

Where equation 9 is the Peppas-Merrill equation, $v_{2,s}$ is the polymer volume fraction in the swollen state, which is calculated from the swelling; $v_{2,r}$ is the polymer volume fraction in the relaxed state, which has been determined from the nominal feed formulation (0.71); \overline{M}_c is the molecular weight between crosslinks; \overline{M}_n is the number average molecular weight of linear polymer chains, which is usually considered large enough to neglect the term $2/\overline{M}_n$, as it has been done here; \bar{v} is the specific volume of the polymer; V_1 is the molar volume of water (18 cm³/mol); χ is the Flory interaction parameter; C_n is the characteristic ratio of the polymer; M_r is

the molecular weight of the repeat unit and l is the bond length of a carbon-carbon bond (1.54 Å). As VP is by far the major component of the polymers, specific volume (0.83 cm³/g), χ (0.48) and C_n (12.3) have been approximated to the values of PVP. M_r has been obtained by weight averaging the molecular weights of the monomers (130 g/mol).

Using this procedure, mesh size values were very similar, in the range 80-90 Å (Table S3).

Table S3. Hydrogel swelling and mechanical properties

Sample	Swelling, S / %	Mesh Size, x / Å	Modulus / MPa	Stress / MPa	Strain / %
VP-ctrl	81.9 ± 0.3	78	0.888 ± 0.081	1.7 ± 0.6	81 ± 2
P2015/VP	82.5 ± 0.2	83	0.589 ± 0.085	0.9 ± 0.1	80 ± 5
P0560/VP	82.7 ± 0.5	85	0.770 ± 0.082	1.1 ± 0.0	81 ± 4
C2030/VP	82.4 ± 0.2	82	0.567 ± 0.071	0.9 ± 0.2	78 ± 14
C2060/VP	82.6 ± 0.4	84	0.368 ± 0.064	1.0 ± 0.0	84 ± 2
C2030-Mo/VP	83.6 ± 0.2	92	0.555 ± 0.032	0.7 ± 0.1	87 ± 10

The surface wettability was measured by using the capillary rise approach.^[26] For that purpose, as depicted in Figure 2D, the hydrogels were fixed on a z-moving part and the water rises due to the capillary effect when in contact with the solution. Interestingly, as has been previously reported, this capillary effect is directly related to the dynamic contact angle.^[27] Contact angle measurements using this procedure can be achieved by measuring the capillary rise (or meniscus height) and introducing the value in the integrated form of the Laplace equation^[28] (see experimental section). This methodology is particularly suited for hydrogels since neither static nor advancing and receding contact angles can be measured by the sessile drop approach. Nevertheless, since hydrogels are extremely hydrophilic the results obtained using this equation lead to values close to 0, independent of the hydrogel analyzed. . For this reason, the capillary rise values (measured in cm) obtained for the different hydrogels have been represented in Figure S9 for the different graphene/hydrogel (VP-Gr) and MoS₂/hydrogel (VP-MoS₂) materials.

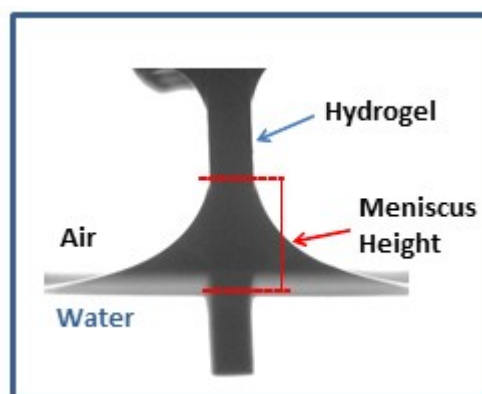


Figure S9. Scheme describing the contact angle measurements by using the capillary rise approach

4. *Experimental protocol for cell culture experiments.*

Prior to cell studies, all hydrogels were sterilized with a 70 % ethanol solution rinsing four times during 10 minutes. Then, they were washed with PBS four times, exposed to UV radiation during 20 minutes, washed two times with incomplete Dulbecco's modified Eagle's medium (DMEM) high in glucose (D6429; Sigma-Aldrich, St. Louis, MO), and finally washed twice with complete culture medium: 10% Fetal Bovine Serum (FBS) (Hyclone®, Thermo Scientific, Waltham, MA) and antibiotics: 100 U/mL penicillin, 100 µg/mL streptomycin sulfate and 0.2 mg/ml G418 (Sigma-Aldrich, St. Louis, MO).

The cell studies were carried out using C166-GFP, a mouse endothelial cell line (CRL 2586™, obtained from ATCC®, USA) derived by transfection with a plasmid reporter vector, pEGFP-N1, encoding enhanced green fluorescent protein (GFP). Routine passaging of the cell line was performed with DMEM high in glucose, supplemented with 10% fetal bovine serum plus antibiotics. As a result of their self-fluorescence, they can be analyzed through some non-opaque/translucent surfaces, such as the hydrogels employed here.

For culturing on the hydrogels, single cells were seeded on the samples with a density of $1,5 \times 10^4 / \text{cm}^2$ in supplemented DMEM. Hydrogels were placed in a 24-well plate in a maintenance medium, and incubated at 37 °C with 5% CO₂ in a humidified incubator. For cell detachment experiments, hydrogels were moved to a new 24-well plate with surface treatment for cell culture and supplemented DMEM, inverting the biomaterial bringing into contact the

cell layer with the plastic TCP surface for at least 4 hours, after which the hydrogels were removed.

Metabolic activity study: Alamar Blue assay.

Metabolic activity of cells was measured by Alamar Blue assay, performed following the manufacturer's instructions (Biosource, CA, USA). Assays were performed in triplicate on each sample type. This method is non-toxic, scalable and uses the natural reducing power of living cells, generating a quantitative measure of cell viability and cytotoxicity. Briefly, Alamar Blue dye (10 % of the culture volume) was added to each well, containing living cells seeded on films, and incubated for 90 minutes. The fluorescence ($\lambda_{\text{ex}}/\lambda_{\text{em}}$ 535/590 nm) of each well was measured using a plate-reader (Synergy HT, Brotek).

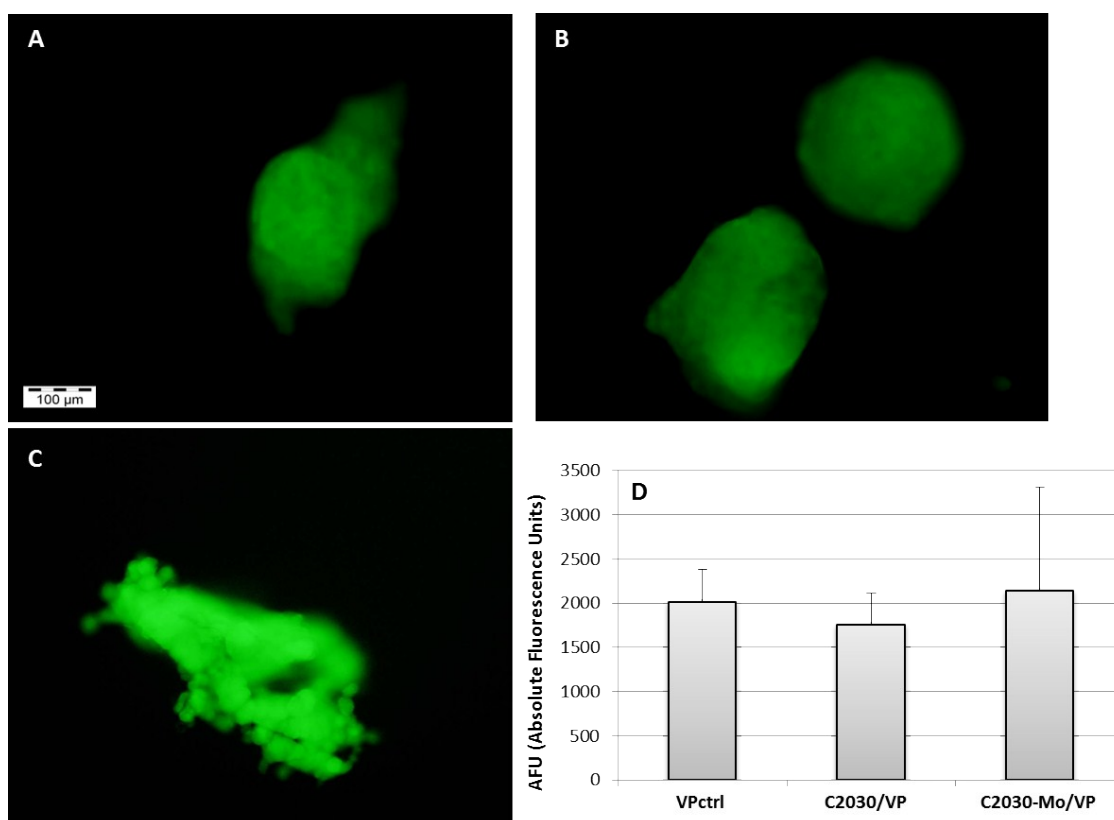


Figure S10. Cell proliferation over VP hydrogels (A) containing graphene (B) and MoS₂ (C) (scale bar in A applies for A to C). Fluorescence images of endothelial C166 GFP cells growing over hydrogel surface at 168 h. (D) Alamar Blue (metabolic activity) of cell culture over hydrogels at 168 h.

Cells grown on the different hydrogels were detached by hydrogel inversion onto a new TCP. After 72 hours, cell monolayers proliferated on the TCP, with no loss of viability, reaching optimal values of metabolic activity. No significant differences were found between samples. A trend can be identified for VP-MoS₂, with a slight increase in the measured fluorescence.

References

- [1] J. N. Coleman, M. Lotya, A. O'Neill, S. D. Bergin, P. J. King, U. Khan, et al. *Science* 2011, 331, 568-71
- [2] Y. Hernandez, V. Nicolosi, M. Lotya, F. M. Blighe, Z. Sun, S. De, Nat. *Nanotech.* 2008, 3, 563
- [3] A. P. S. Gaur, S. Sahoo, M. Ahmadi, S. P. Dash, M. J.-F. Guinel, and R. S. Katiyar *Nano Lett.*, 2014, 14, 4314
- [4] Y. Hernandez, M. Lotya, D. Rickard, S. D. Bergin, J. N. Coleman, *Langmuir*, 2010, 26, 3208
- [5] J. N. Coleman, *Acc. Chem. Res.* 2013, 46, 14
- [6] G. Cunningham, M. Lotya, C. S. Cucinotta, S. Sanvito, S. D. Bergin, R. Menzel et al. *ACS Nano*, 2012, 6, 3468
- [7] G. Eda, H. Yamaguchi, D. Voiry, T. Fujita, M. Chen, M. Chhowalla, *NanoLett.* 2011, 11, 5111.
- [8] C. Lee, H. Yan, L. E. Brus, T. F. Heinz, J. Hone, S. Ryu, *ACS Nano*, 2010, 4, 2695.
- [9] L. G. Cançado, L.G. K. Takai, T. Enoki, M. Endo, Y. A. Kim, H. Mizusaki et al. *Appl. Phys. Lett.* 2006, 88, 163106.
- [10] Z. Sun, J. Vivekananthan, D. A. Guschin, X. Huang, V. Kuznetsov, P. Ebbinghaus, et al. *Chem. Eur. J.* 2014, 20, 5752 – 5761
- [11] L. G. Cançado, A. Jorio, E. H. Martins Ferreira, F. Stavale, C. A. Achete, R. B. Capaz et al. *Nano Lett.* 2011, 11, 3190
- [12] C. Backes, K. R. Paton, D. Hanlon, S. Yuan, M. I. Katsnelson, J. Houston, et al. *Nanoscale* 2016, 8, 4311.
- [13] R. Feng, C. Wang, X. Xu, F. Yang, G. Xu and T. Jiang, *Journal of Membrane*

Science, 2011, 369, 233-242.

[14] C. R. Kinnane, G. K. Such, G. Antequera-García, Y. Yan, S. J. Dodds, L. M. Liz-Marzan and F. Caruso, *Biomacromolecules*, 2009, 10, 2839-2846.

[15] P. Kanagaraj, A. Nagendran, D. Rana, T. Matsuura, S. Neelakandan and K. Malarvizhi, *Industrial & Engineering Chemistry Research*, 2015, 54, 4832-4838.

[16] E. M. Ahmed, *Journal of Advanced Research*, 2015, 6, 105-121.

[17] I. Aranaz, E. Martinez-Campos, M. E. Nash, M. G. Tardajos, H. Reinecke, C. Elvira, V. Ramos, J. Luis Lopez-Lacomba and A. Gallardo, *Journal of Materials Chemistry B*, 2014, 2, 3839-3848.

[18] H. Reinecke and A. Gallardo, *Macromolecular Theory and Simulations*, 2009, 18, 25-29.

[19] J. P. Gong, Y. Katsuyama, T. Kurokawa and Y. Osada, *Advanced Materials*, 2003, 15, 1155-1158.

[20] A. Flores, H. J. Salavagione, F. Ania, G. Martinez, G. Ellis and M. A. Gomez-Fatou, *Journal of Materials Chemistry C*, 2015, 3, 1177-1180

[21] D. Y. Kwok, C. J. Budziak and A. W. Neumann, *Journal of Colloid and Interface Science*, 1995, 173, 143-150.

[22] D. Quéré and J.-M. Di Meglio, *Advances in Colloid and Interface Science*, 1994, 48, 141-150.

[23] Y. Yuan and T. R. Lee, in *Surface Science Techniques*, eds. G. Bracco and B. Holst, Springer Berlin Heidelberg, 2013, vol. 51, pp. 3-34.

[24] J. B. Cain, D. W. Francis, R. D. Venter and A. W. Neumann, *Journal of Colloid and Interface Science*, 1983, 94, 123-130.

[25] D.A. Carr, N.A. Peppas, *Macromol.Biosci.* 2009, 9, 497

[26] D. Y. Kwok, C. J. Budziak, A. W. Neumann, *Journal of Colloid and Interface Science* 1995, 173, 14

[27] D. Quéré, J.-M. Di Meglio, *Advances in Colloid and Interface Science* 1994, 48, 141; Y. Yuan, T. R. Lee, in *Surface Science Techniques*, Vol. 51 (Eds: G. Bracco, B. Holst), Springer Berlin Heidelberg, 2013, 3

[28] J. B. Cain, D. W. Francis, R. D. Venter, A. W. Neumann, *Journal of Colloid and Interface Science* 1983, 94, 123.